



Reanalyzing the upper limit on the tensor-to-scalar perturbation ratio r_T in a quartic potential inflationary model



R. Kabir*, A. Mukherjee, D. Lohiya

Department of Physics and Astrophysics, University of Delhi, Delhi 110007, India

ARTICLE INFO

Article history:

Received 1 June 2014

Received in revised form 14 July 2014

Accepted 18 July 2014

Available online 23 July 2014

Editor: S. Dodelson

ABSTRACT

We study the polynomial chaotic inflation model with a single scalar field in a double well quartic potential which has recently been shown to be consistent with Planck data. In particular, we study the effects of lifting the degeneracy between the two vacua on the inflationary observables, i.e., spectral index n_s and tensor-to-scalar perturbation ratio r_T . We find that removing the degeneracy allows the model to satisfy the upper limit constraints on r_T from Planck data, provided the field starts near the local maximum. We also calculate the scalar power spectrum and non-Gaussianity parameter f_{NL} for the primordial scalar perturbations in this model.

© 2014 The Authors. Published by Elsevier B.V. This is an open access article under the CC BY license (<http://creativecommons.org/licenses/by/3.0/>). Funded by SCOAP³.

1. Introduction

Inflation is regarded as the standard cosmological paradigm to describe the physics of the very early Universe. It leads to a causal mechanism to generate almost scale invariant fluctuations on cosmological scales, with small deviations that follow from the precise microphysics of inflation. This prediction is consistent with the recently announced measurements of the cosmic microwave background (CMB) anisotropies by the Planck satellite. The latest data allow us to constrain the inflationary model besides giving a slightly red tilted spectral index $n_s = 0.9603 \pm 0.0073$, ruling out exact scale invariance $n_s = 1$ at over 5σ [1]. The Planck data also provide observational bounds on primordial non-Gaussianity parameter, i.e., local $f_{NL} = 2.7 \pm 5.8$ at 68% confidence level for the reduced bispectrum [2].

Just after Planck results were announced, different scalar potentials were revisited to explore concordance with these results [1]. The data reinforced the ruling out of single-field inflationary models $V(\phi) = \phi^n$ with $n \geq 2$, which were already disfavored or marginally disfavored by WMAP. (This does not apply to alternative inflationary scenarios e.g., warm inflation [3].) However Croon et al. [4] demonstrated that the double well degenerate potential $V(\phi) = A\phi^2(v^2 - 2vB\phi + \phi^2)$ is consistent with Planck data, although with severe constraints on the initial condition for ϕ and on the allowed range of B . The polynomial quartic potential with

double well is the most studied potential in a variety of settings. It is also well motivated by the physics beyond the Standard Model, viz. supergravity and superstring theories [5]. The characteristic interesting features [4,6] of the potential have been the primary motivation for a lot of effort to explore its consistency with the Planck data [1].

2. Basic formalism

2.1. Slow roll parameters

We review the formalism in [4] to set up our notation. For an inflationary model described by the potential $V(\phi) = A\phi^2(v^2 - 2vB\phi + \phi^2)$, the slow-roll parameters are defined as

$$\epsilon \equiv \frac{1}{2} M_{\text{pl}}^2 \left(\frac{V_\phi}{V} \right)^2 = 2M_{\text{pl}}^2 \frac{(v^2 - 3vB\phi + 2\phi^2)^2}{\phi^2(v^2 - 2vB\phi + \phi^2)^2}, \quad (1)$$

$$\eta \equiv M_{\text{pl}}^2 \left(\frac{V_{\phi\phi}}{V} \right) = 2M_{\text{pl}}^2 \frac{(v^2 - 6vB\phi + 6\phi^2)}{\phi^2(v^2 - 2vB\phi + \phi^2)} \quad (2)$$

and

$$\begin{aligned} \xi &\equiv M_{\text{pl}}^4 \left(\frac{V_\phi V_{\phi\phi\phi}}{V^2} \right) \\ &= 24M_{\text{pl}}^4 \frac{(-vB + 2\phi)(v^2 - 3vB\phi + 2\phi^2)}{\phi^3(v^2 - 2vB\phi + \phi^2)^2} \end{aligned} \quad (3)$$

where

$$V_\phi \equiv \frac{dV}{d\phi}, \quad V_{\phi\phi} \equiv \frac{d^2V}{d\phi^2} \quad \text{and} \quad V_{\phi\phi\phi} \equiv \frac{d^3V}{d\phi^3}. \quad (4)$$

* Corresponding author.

E-mail addresses: rakesh@physics.du.ac.in (R. Kabir), am@physics.du.ac.in (A. Mukherjee), dlohiya@physics.du.ac.in (D. Lohiya).

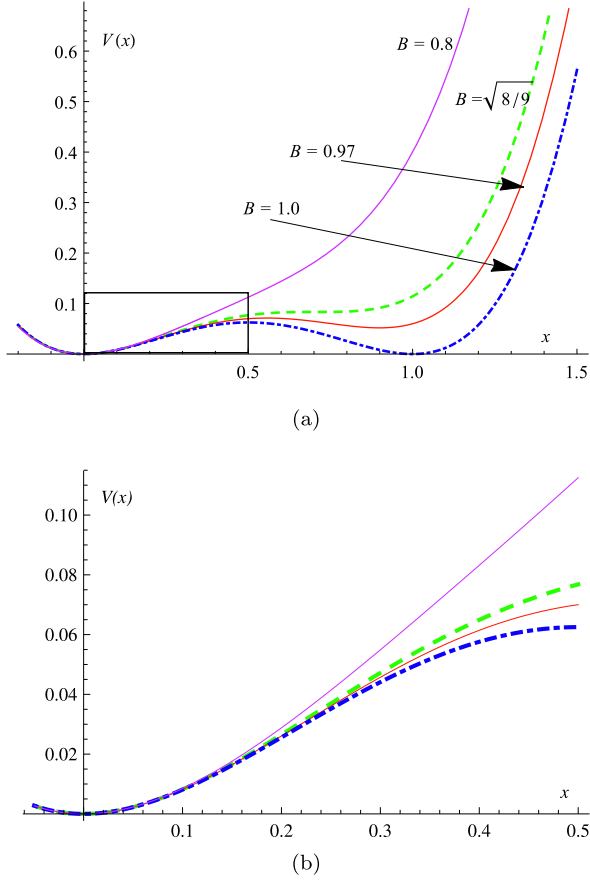


Fig. 1. (a) An illustration of the potential for different values of B ; (b) Inset in (a) zoomed to highlight the behavior as $x \rightarrow 0^+$.

In terms of the slow-roll parameters, the scalar spectral index is expressed as

$$n_s = 1 - 6\epsilon + 2\eta \quad (5)$$

and the tensor-to-scalar ratio as

$$r_T = 16\epsilon. \quad (6)$$

Finally the number of e-folds is given by

$$N = -\frac{1}{M_{\text{pl}}^2} \int_{\phi_i}^{\phi_e} \left(\frac{V}{V_\phi} \right) d\phi \quad (7)$$

where $\phi_{e,i}$ are the values of ϕ at the end and beginning of the inflationary epoch.

The scalar power spectrum $P_s(k)$ is described in terms of the spectral index $n_s(k)$ by

$$P_s(k) = A \exp \left[(n_s - 1) \ln(k/k_0) + \frac{1}{2} \alpha_s \ln^2(k/k_0) \right] \quad (8)$$

where

$$\alpha_s \equiv \frac{dn_s}{d \ln k} \quad (9)$$

which in terms of slow-roll parameters is

$$\alpha_s = \frac{1}{8\pi^2} \left[-\frac{\xi}{4} + 2\eta\epsilon - 3\epsilon^2 \right]. \quad (10)$$

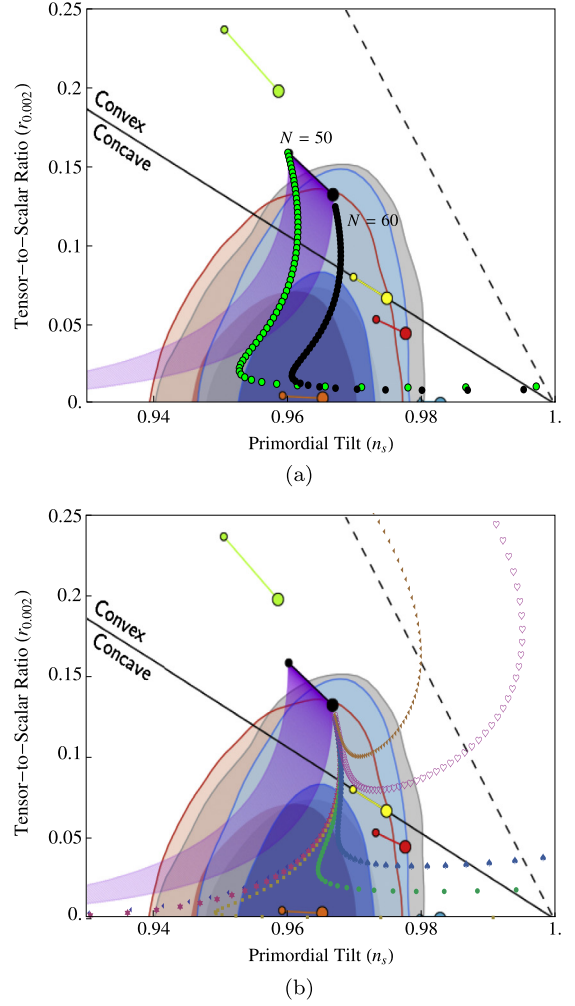


Fig. 2. The reproduction of the work by Nakayama et al. [5]. (a) The two curves correspond to $N = 50$ (green) and 60 (black). Each curve is generated by varying x_i from 0.005 to 1.0 in steps of 0.012 . In this plot we have fixed $B = 0.93$ for both curves. (b) The seven curves correspond to B : $0.96, 0.95, 0.94, 0.92, 0.90, 0.80, 0.70$ for $N = 60$. Each curve is again generated by varying x_i as in (a). (For interpretation of the references to color in this figure legend, the reader is referred to the web version of this article.)

2.2. Inflaton potential and background dynamics

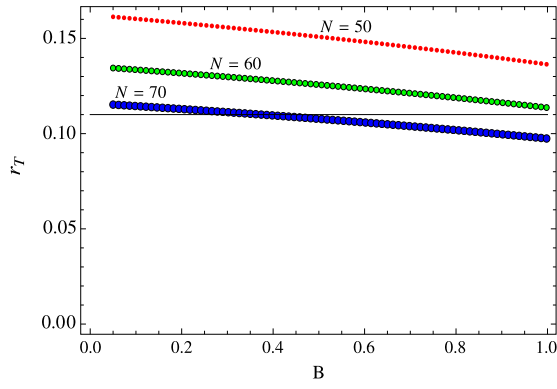
On parameterizing the field as $\phi \rightarrow xv$, where x is dimensionless, for the chosen potential in [4], the inflationary observables reduce to¹:

$$\epsilon = \frac{2M_{\text{pl}}^2(1 + 2x^2 - 3xB)^2}{v^2x^2(1 + x^2 - 2xB)^2}, \quad (11)$$

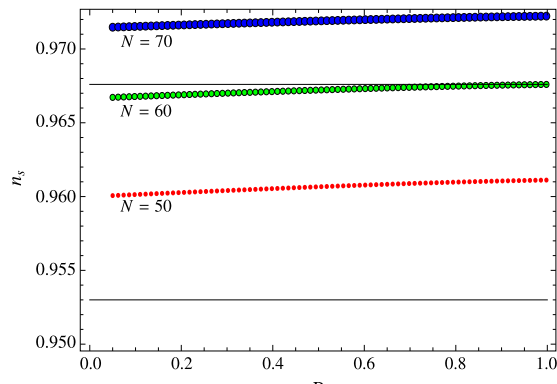
$$\eta = \frac{2M_{\text{pl}}^2(1 + 6x(x - B))}{v^2x^2(1 + x^2 - 2xB)}, \quad (12)$$

$$\xi = \frac{24M_{\text{pl}}^4(2x - B)(1 + 2x^2 - 3xB)}{v^4x^3(1 + x^2 - 2xB)^2} \quad (13)$$

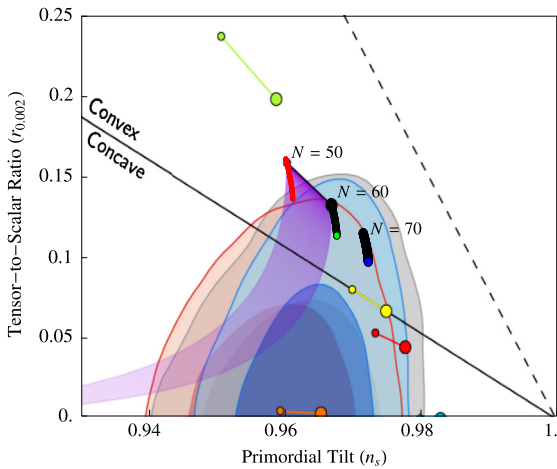
¹ In [4], a minus sign is missing in the expression for N . Further, the power of $(1 - x)$ in their Eq. (10), generalized in our Eq. (13), should be 4 and not 2. This error creeps into the numerical calculation (in table) also. A summary of standard formulae can be found in [7].



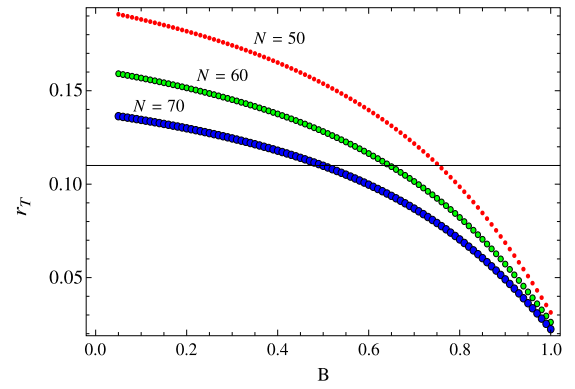
(a)



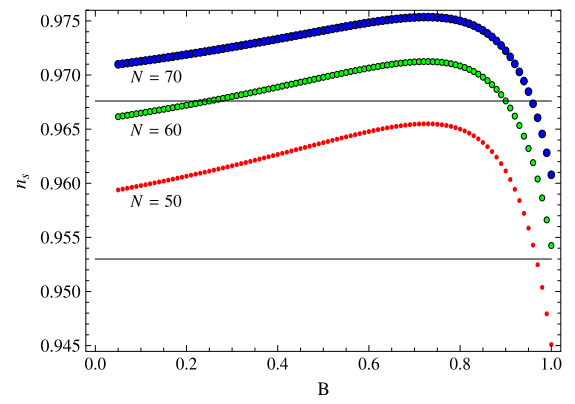
(b)



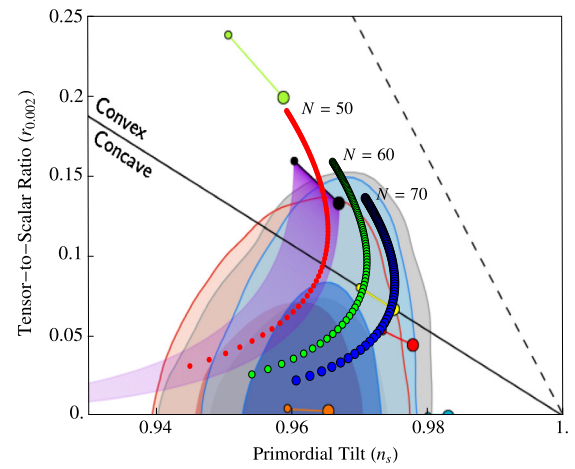
(c)



(a)



(b)



(c)

Fig. 3. (a) The tensor-to-scalar perturbation ratio r_T as a function of B for $N = 50$ (red), 60 (green) and 70 (blue). In this plot we have taken $x_i = 0.1$ for all three curves. The horizontal line shows the upper limit for $r_T = 0.11$. (b) Spectral index n_s as a function of B with the same color coding as in (a). Two horizontal lines show the constraint on n_s , i.e., $n_s = 0.9603 \pm 0.0073$. (c) Prediction in the (n_s, r_T) plane corresponding to (a) and (b). For example, each red point in the (n_s, r_T) plane corresponds to a value of r_T (red point in (a)) and a value of n_s (red point in (b)), both calculated for a particular value of B . (For interpretation of the references to color in this figure legend, the reader is referred to the web version of this article.)

and

$$N = -\frac{v^2}{M_{\text{pl}}^2} \int_{x_i}^{x_e} \left(\frac{V}{V_x} \right) dx. \quad (14)$$

We point out that the range of possible initial field values is severely restricted if $B > \sqrt{8/9}$, as the integral for N will not con-

Fig. 4. Same as in Fig. 3, but here we have taken $x_i = 0.4$ (near the local maximum) for all three curves. Note the characteristic interesting behavior when field starts near the local maximum. (For interpretation of the references to color in this figure legend, the reader is referred to the web version of this article.)

verge on choosing an initial field value beyond the local maximum (see Fig. 6). This rules out the possibility of investigation of deviation from slow-roll or multiphase-inflation. Punctuated inflation [6] is the simplest and interesting example of multi-phase-inflation which occurs in our model when $B \sim \sqrt{8/9}$ and the initial field value is chosen beyond the point of inflection.

We now explore the behavior of the inflationary observables, including $P_s(k)$ and f_{NL} as B is varied from 1 to 0 within the slow-roll regime. Our analysis suggests a broad range of B for which prediction in the (n_s, r_T) plane lies within the 1σ level.

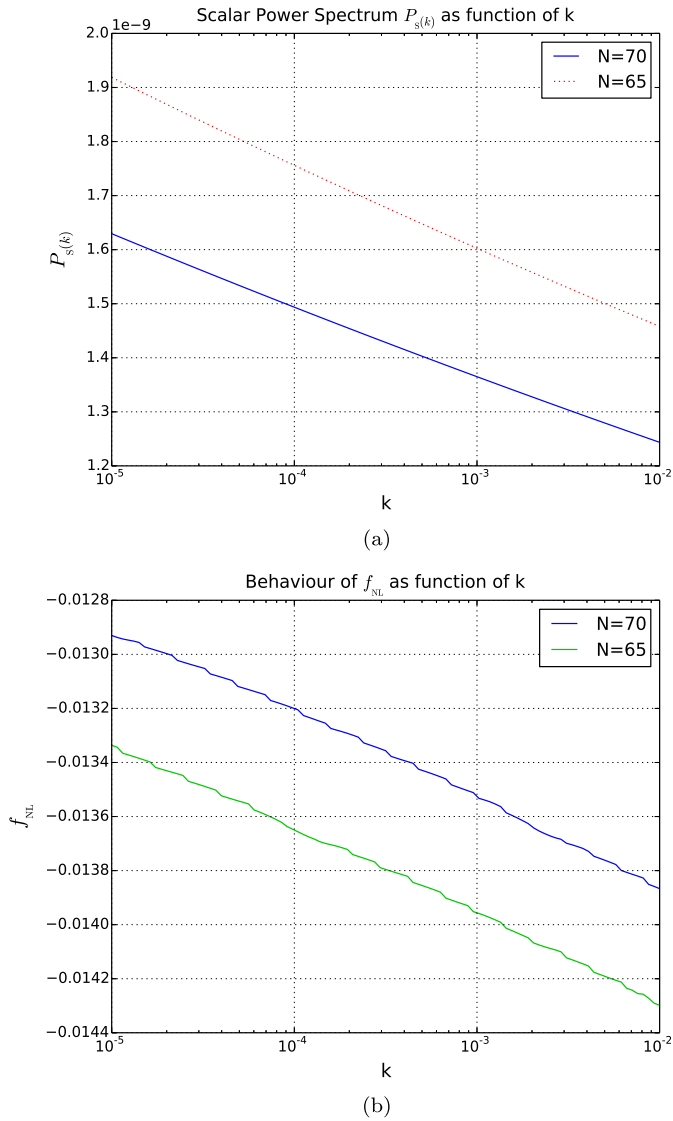


Fig. 5. (a) The scalar power spectrum as a function of k plotted on a logarithmic scale for $B = 0.96$ and $x_i = 0.4$ over two e-folds. (b) A plot of f_{NL} as a function of k on a logarithmic scale. The values of B and x_i are the same as in (a).

2.3. Discussion about the potential shape

The global shape of the potential depends on the coefficient B as shown in Fig. 1. For $B = 1$, there is one local maximum at $x = 0.5$ and two degenerate minima at $x = 0$ and 1.0 . For $B < 1.0$, the minimum at $x = 1.0$ is lifted. As long as there is such a local maximum, the initial value of the inflaton field should be below the local maximum since otherwise the inflaton would be trapped in the false vacuum.

The false vacuum disappears for $B < \sqrt{8/9}$. Interestingly, if B marginally satisfies the inequality, there appears a flat plateau at around the point of inflection. If one starts at a suitable value of the field beyond the point of inflection in the above potential, it is found that one can achieve two epochs of slow roll inflation sandwiching a brief period of departure from inflation (lasting for a little less than one e-fold), a scenario which has been dubbed as punctuated inflation [6]. In fact, it is the point of inflection, around which the potential exhibits a plateau with an extremely small curvature, which permits such an evolution to be possible.

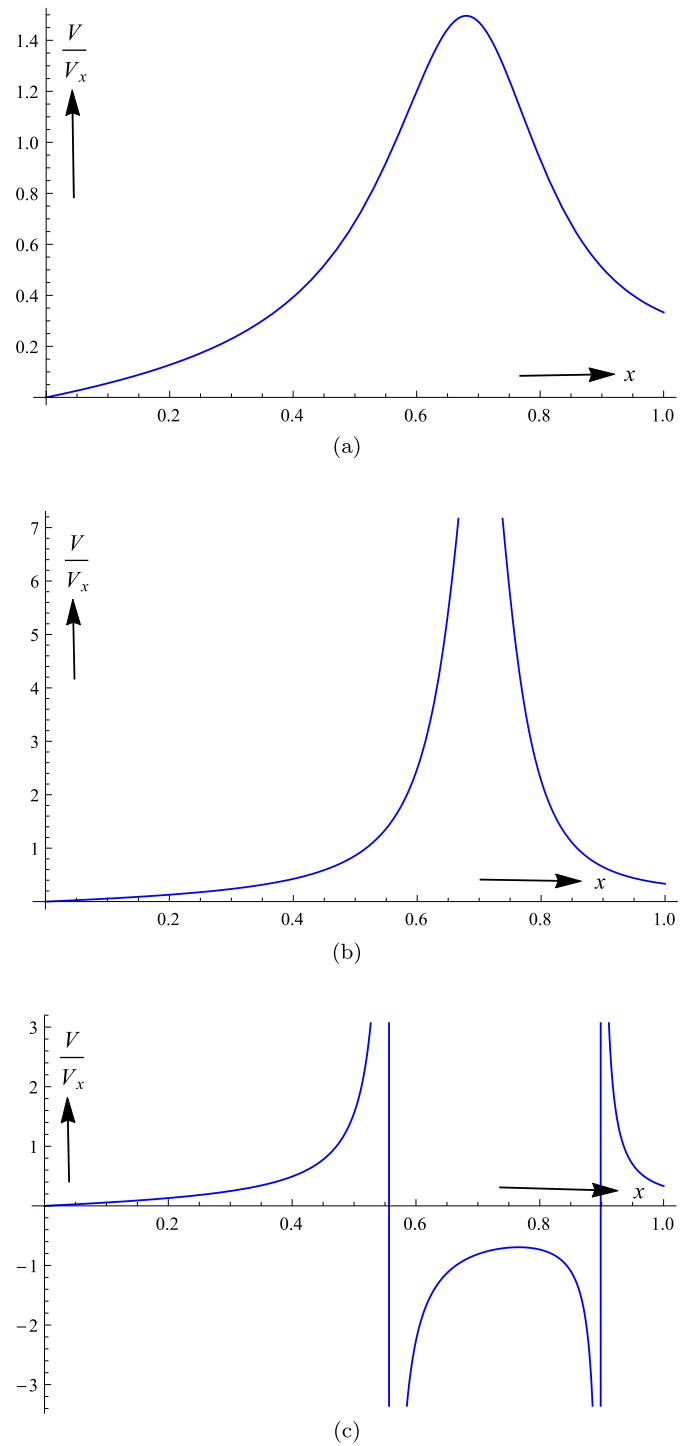


Fig. 6. Schematic plot of integrand for N for (a) $B = 0.92$, (b) $B = 0.94$ and (c) $B = 0.97$; see Eq. (14).

It needs to be kept in mind that this potential does not provide a single inflation model, but rather a class of the inflationary models as we vary B from 0 to 1. Fig. 1 describes the potential profile for four values of B . Interestingly, there are two ways to mimic the quadratic potential case: (a) by changing the class of potential by decreasing B from 1 to 0 and (b) by taking the initial field value very near to zero (near the first minimum) [4]. However, as shown in Fig. 1b, each member of the class is asymptotic to the quadratic case if $x_i < 0.12$ irrespective of the value of B .

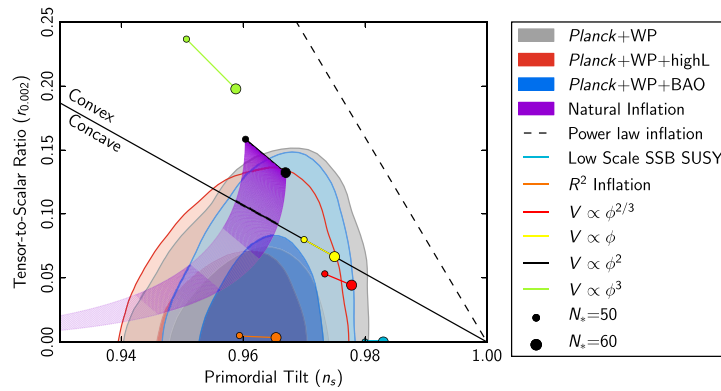


Fig. 7. Marginalized joint 68% and 95% CL regions for n_s and $r_{0.002}$. Observational 1σ (dark) and 2σ (light) constraints from the Planck satellite [1] are also shown: Planck + WMAP polarization (gray), Planck + WMAP polarization + high- ℓ CMB measurement (red), Planck + WMAP polarization + baryon acoustic oscillation (blue). Filled circles connected by line segments show the predictions from chaotic inflation with $V \propto \phi^3$ (green), ϕ^2 (black), ϕ (yellow), $\phi^{2/3}$ (red) and R^2 inflation (orange), for $N = 50$ (small circle) – 60 (big circle). The purple band shows the prediction of natural inflation [1]. (For interpretation of the references to color in this figure legend, the reader is referred to the web version of this article.)

3. Numerical results

We set out to explore the model for the entire range of B values from 0 to 1 and for an arbitrary initial field value ϕ_i (or equivalently x_i). We need to keep in mind that an arbitrary large initial field value can be taken only for those members of the class for which $B < \sqrt{8/9}$, otherwise either deviation from slow roll will occur (when $B = \sqrt{8/9}$) or the field will be trapped in the false vacuum (when $B > \sqrt{8/9}$).

3.1. Prediction in (n_s, r_T) plane

Fig. 3 exhibits how our analysis differs from the past work of Nakayama et al. [5] (see Fig. 2), where effects mainly due to varying initial field value are considered. In contrast, we have varied B continuously for each fixed initial field value—from the one near the minimum at $x = 0$ to the other near the local maximum—and for three e-fold values: $N = 50, 60$ and 70 . However, we have shown the analysis only for the two extreme initial field values because of clarity and reasons of space (see Figs. 3 and 4).

Plots only on the (n_s, r_T) plane, as done in [5], hide valuable information of initial conditions for which the model lies within 1σ . Notice that very near to $x = 0.005$, predictions (i.e., points in the (n_s, r_T) plane) start from the quadratic potential (the black line), found concordant with the Planck data, and then graze the contour as x is increased; see Figs. 2 and 7.

From Fig. 3a, it is clear that for $N = 50$ (red) and 60 (green), this model is completely above the bound imposed by Planck ($r_T < 0.11$) for the entire range of B —here the field starts near the origin; whereas for $N = 70$ (blue), the model is at the margin of this bound.

When we contrast the above situation with Fig. 4a, we find that the upper limit on r_T is satisfied for sufficiently large values of B (red and green curves fall below the horizontal line for $B \gtrsim 0.75$ and $B \gtrsim 0.65$ respectively). It is emphasized that this is the case when the field starts near the local maximum ($x \sim 0.4$). Fig. 4c makes this explicit, showing that even a part of the red curve ($N = 50$) is within 1σ of the Planck value. Although there is no appreciable disagreement between Planck and BICEP2 results as clarified in [8], a slightly larger tensor-to-scalar ratio ($r_T \sim 1.6$), as required by BICEP2, is within reach (e.g., when $B \sim 0.3$) as shown in Fig. 4a. Another way to realize a large r_T is by assuming the non-monotonicity of the slow-roll parameter ϵ , as considered in a model somewhat similar to ours [9].

3.2. Non-Gaussianity

Non-Gaussianity is now a standard cosmological observable, comparable to the spectral index (n_s) and tensor-to-scalar ratio r_T , and is a powerful discriminant between competing models. It is therefore desirable to study aspects of non-Gaussianity for this model too. We have numerically calculated the equilateral limit of the local f_{NL} parameter [10]. In Fig. 5a, the power spectrum is plotted as a function of k , from which it is clear that the spectrum is not scale invariant on any scale (otherwise it would have been a horizontal straight line). In Fig. 5b, the non-Gaussianity parameter f_{NL} is plotted as a function of k , from which we observe that the very low values of $|f_{NL}|$ (~ 0.01) lie in the range predicted by Planck data for local $f_{NL} = 2.7 \pm 5.8$ [2]. The very small non-Gaussianity, inferred from BICEP2 data owing to comparatively larger r_T [11] (see also [12]), is compatible with our results also [13]. This observation is also consistent with the fact that single-field slow roll models predict a very small non-Gaussianity [14].

4. Summary and conclusion

In this letter, we have explored in detail the (B, ϕ_i) space within the slow-roll regime for the quartic potential. We have explicitly shown that on varying B , interesting patterns on the variation of n_s and r_T arise *only* when field dynamics captures the deviation from the quadratic case, i.e., the field should start near the local maximum, not near the origin. Even though this parameter space has been moderately studied in [5], the authors restricted their analysis to a few discrete values of B . Similarly Ellis et al. [15] have carried out a statistical study with just four explicit values of numerical coefficient in a two field model to explore concordance with the preferred observational values of n_s and r_T .

One of the main well-known problems—constraints from Planck on the upper limit on r_T —has been reanalyzed here and we find that there is no respite for the model *solely* due to removing degeneracy between the vacua. On the other hand, merging variations of B with the field starting *near* the local maximum, the model's predictions for (n_s, r_T) lie well within 1σ for a large part of the (B, ϕ_i) space (see Fig. 4). Further, our Fig. 4a clearly shows that large r_T can be generated when the potential is non-degenerate and the field starts near the local maximum. On non-Gaussianity aspects (which were not considered in previous works [4,5]), we have explicitly calculated the local f_{NL} parameter for each mode of our interest and verified that this model indeed

satisfies the constraint imposed by Planck data on non-Gaussianity [2], and is compatible with BICEP2 measurements.

Acknowledgements

R.K. thanks Dheeraj Kumar Hazra for useful communication and Tarun Choudhari for assistance with Latex. We are grateful to Rudnei O. Ramos and Sayantan Choudhury for pointing out their works [3,9,12] respectively. We also thank an anonymous reviewer whose comments helped us highlight the subtle points of our study. The work of R.K. was partially supported by CSIR, New Delhi with the award of JRF (No. 09/045(0930)/2010-EMR-I).

Appendix A

In Fig. 6, we plot the integrand for N for 3 values of B . (As already mentioned, one minimum disappears if $B < \sqrt{8/9} = 0.9428$.) We can clearly see how a discontinuity in $\frac{V}{V_x}$ develops as B increases above $\sqrt{8/9}$. One cannot take any point on the x axis beyond the local maximum, which is near $x = 0.5$ with a slight variation as we change B (see Fig. 1).

Fig. 7 is from Planck Data on which we superimpose our predictions—following [4] and [5].

References

- [1] Planck Collaboration, P.A.R. Ade, Planck 2013 results. XXII. Constraints on inflation, arXiv:1303.5082.
- [2] Planck Collaboration, P.A.R. Ade, Planck 2013 results. XXIV. Constraints on primordial non-gaussianity, arXiv:1303.5084 [astro-ph].
- [3] R.O. Ramos, L.A. da Silva, Power spectrum for inflation models with quantum and thermal noises, J. Cosmol. Astropart. Phys. 2013 (03) (2013), <http://dx.doi.org/10.1088/1475-7516/2013/03/032>, 032–032, arXiv:1302.3544 [astro-ph.CO].
- [4] D. Croon, J. Ellis, N.E. Mavromatos, Wess–Zumino inflation in light of planck, Phys. Lett. B 724 (2013) 165, arXiv:1303.6253 [astro-ph.CO].
- [5] K. Nakayama, F. Takahashi, T.T. Yanagida, Polynomial chaotic inflation in the planck era, Phys. Lett. B 725 (2013) 111, arXiv:1303.7315 [hep-ph].
- [6] R.K. Jain, P. Chingangbam, J.-O. Gong, L. Sriramkumar, T. Souradeep, Punctuated inflation and the low CMB multipoles, J. Cosmol. Astropart. Phys. 2009 (01) (2009), <http://dx.doi.org/10.1088/1475-7516/2009/01/009>, 009, 00049, <http://iopscience.iop.org/1475-7516/2009/01/009>.
- [7] E.W. Kolb, M.S. Turner, The Early Universe, Addison–Wesley, Reading, MA, 1990.
- [8] B. Audren, D.G. Figueroa, T. Tram, A note of clarification: BICEP2 and planck are not in tension, arXiv:1405.1390 [astro-ph].
- [9] S. Choudhury, A. Mazumdar, An accurate bound on tensor-to-scalar ratio and the scale of inflation, Nucl. Phys. B 882 (2014) 386–396, <http://dx.doi.org/10.1016/j.nuclphysb.2014.03.005>, <http://www.sciencedirect.com/science/article/pii/S0550321314000790>.
- [10] D.K. Hazra, L. Sriramkumar, J. Martin, BINGO: a code for the efficient computation of the scalar bi-spectrum, J. Cosmol. Astropart. Phys. 2013 (05) (2013), <http://dx.doi.org/10.1088/1475-7516/2013/05/026>, 026–026, arXiv:1201.0926 [astro-ph].
- [11] G. D’Amico, M. Kleban, Non-gaussianity after BICEP2, arXiv:1404.6478 [astro-ph].
- [12] S. Choudhury, A. Mazumdar, Reconstructing inflationary potential from BICEP2 and running of tensor modes, arXiv:1403.5549 [astro-ph].
- [13] D.K. Hazra, A. Shafieloo, G.F. Smoot, A.A. Starobinsky, Whipped inflation, arXiv:1404.0360 [astro-ph].
- [14] J. Maldacena, Non-gaussian features of primordial fluctuations in single field inflationary models, J. High Energy Phys. 2003 (05) (2003), <http://dx.doi.org/10.1088/1126-6708/2003/05/013>, 013–013, 01332, arXiv:astro-ph/0210603.
- [15] J. Ellis, N.E. Mavromatos, D.J. Mulryne, Exploring two-field inflation in the Wess–Zumino model, arXiv:1401.6078 [astro-ph].